Atmos. Chem. Phys. Discuss., 9, 8223–8260, 2009
www.atmos-chem-phys-discuss.net/9/8223/2009/
© Author(s) 2009. This work is distributed under
the Creative Commons Attribution 3.0 License.

Atmospheric Chemistry and Physics Discussions

This discussion paper is/has been under review for the journal *Atmospheric Chemistry and Physics (ACP)*. Please refer to the corresponding final paper in *ACP* if available.

New particle formation from the oxidation of direct emissions of pine seedlings

L. Q. Hao[1], P. Yli-Pirilä[2], P. Tiitta[1], S. Romakkaniemi[1], P. Vaattovaara[1], M. K. Kajos[3], J. Rinne[3], J. Heijari[2], A. Kortelainen[1], P. Miettinen[1], J. H. Kroll[4], J.-K. Holopainen[2], J. Joutsensaari[1], M. Kumala[3], D. R. Worsnop[4], and A. Laaksonen[1,5]

[1]Department of Physics, University of Kuopio, Kuopio 70211, Finland
[2]Department of Environmental Sciences, University of Kuopio, Kuopio 70211, Finland
[3]Department of Physics, P.O. Box 68, University of Helsinki, Helsinki 00014, Finland
[4]Aerodyne Research, Inc., Billerica, MA, 08121-3976, USA
[5]Finnish Meteorological Institute, Helsinki 00101, Finland

Received: 11 March 2009 – Accepted: 16 March 2009 – Published: 27 March 2009

Correspondence to: L. Q. Hao (liqing@uku.fi)

Published by Copernicus Publications on behalf of the European Geosciences Union.

Abstract

Measurements of particle formation following the gas phase oxidation of volatile organic compounds (VOCs) emitted by Scots pine (*Pinus sylvestris L.*) seedlings are reported. Particle nucleation and condensational growth both from ozone (O_3) and hydroxyl radical (OH) initiated oxidation of pine emissions (about 20–120 ppb) were investigated in a smog chamber. During experiments, tetramethylethylene (TME) and 2-butanol were added to control the concentrations of O_3 and OH. Particle nucleation and condensational growth rates were interpreted with a chemical kinetics model. Scots pine emissions mainly included α-pinene, β-pinene, Δ^3-carene, limonene, myrcene, β-phellandrene and isoprene, composing more than 95% of total emissions. Modeled OH concentration in the O_3+OH induced experiments was at a level of $\sim 10^6$ molecular cm^{-3}. Our results demonstrate that OH-initiated oxidation of VOCs plays an important role in the nucleation process during the initial new particle formation stage. The highest average nucleation rate of 360 $cm^{-3}\,s^{-1}$ was observed for the OH-dominated nucleation events and the lowest aerosol mean formation rate less than 0.5 $cm^{-3}\,s^{-1}$ for the case with only O_3 present as an oxidant. On the other hand, ozonolysis of monoterpenes appears to be much more efficient to the aerosol growth process following nucleation. Higher contributions of more oxygenated products to the SOA mass loadings from OH-dominating oxidation systems were found as compared to the ozonolysis systems. Comparison of mass and volume distributions from the aerosol mass spectrometer and differential mobility analyzer yields estimated effective density of these SOA to be 1.34±0.06 g cm^{-3} with the OH plus O_3 initiated oxidation systems and 1.38±0.03 g cm^{-3} with the ozonolysis dominated chemistry.

1 Introduction

On the worldwide basis, the annual biogenic VOCs flux is estimated to be in the range of 491∼1150 Tg C (Guenther et al., 1995; Griffin et al., 1999). These biogenic VOCs re-

act with O_3, OH and nitrate radical (NO_3), leading to the formation of secondary organic aerosols (SOA). Globally, the annual SOA production from these biogenic precursors is estimated to range from 2.5 to 44.5 Tg C (Tsigaridis and Kanakidou, 2003), composing about 60% of the organic aerosol mass on the global scale and even higher fraction regionally (Kanakidou et al., 2005). SOA can directly affect the Earth's radiation budget by scattering and absorbing incoming solar radiation. Additionally, SOA can affect indirectly the radiation budget by modifying cloud properties through its potential contribution to the population of cloud condensation nuclei (CCN). SOA particles may also have adverse effects on human health through their inhalation. Understanding these effects requires a greater knowledge of the mechanisms inducing aerosol formation in the atmosphere.

Monoterpenes and isoprene are important classes of globally emitted organic biogenic species. Their oxidation leads to low volatile products (low saturation vapor pressure) which are believed to be able to nucleate once their saturation ratio increased sufficiently. Compounds with higher saturation pressure, known as semi-volatile organic compounds, will partition into the previously formed particle phase, contributing to the growth and mass loadings of atmospheric aerosols. Thus, the SOA formation from oxidation of monoterpenes (Hoffmann et al., 1997; Jang and Kamens, 1999; Gao et al., 2004; Shilling et al., 2008; Presto and Donahue, 2005; Odum et al., 1996; Yu et al., 1999) and isoprene (Ng et al., 2007; Kroll et al., 2006; Claeys et al., 2004) by OH, O_3 and NO_3 has been intensively studied in laboratory and field campaigns (e.g. Kulmala et al., 2004; Laaksonen et al., 2008, etc.). These studies have demonstrated that atmospheric oxidation of monoterpenes and isoprene represents significant source of SOA. Despite the important advances that have been made in SOA studies, the SOA formation in the atmosphere is still poorly understood. For example, the roles OH and O_3 play in the SOA formation is still partially unknown and the conclusions made to this point in previous studies are somewhat contradictory. Bonn and Moortgat (2002) and Koch et al. (2000) concluded that OH oxidation of monoterpenes in the atmosphere is not an important source of new SOA particles, whereas Burkholder et al. (2007)

reported that OH initiated oxidation allows for nucleation. Moreover, in chamber studies, only a single organic precursor was usually employed as a model compound to simulate the SOA formation in any given experiment. Since the mechanisms of SOA formation from oxidation of biogenic hydrocarbons are complex, it is uncertain into what degree the results from the single monoterpene chamber studies can be extrapolated to the conditions prevailing in the real atmosphere (VanReken et al., 2006). Recent studies have started to address these types of questions. In these studies, aerosol formation events were simulated in more realistic conditions by using the direct biogenic emissions of macroalgae (McFiggans et al., 2004), white cabbage (Joutsensaari et al., 2005; Pinto et al., 2007), oak and loblolly pine (VanReken et al., 2006) and birch/pine/spruce emissions (Mentel et al., 2009). In some of these studies, new particle formation efficiencies from OH- or O_3-induced oxidation was also investigated.

In this study we concentrate on the aerosol particle nucleation in a laboratory using direct VOCs emissions of living Scots pine seedlings. Scots pine was selected because it is one of the dominant tree species in the European boreal forest (Räisänen et al., 2008). Both O_3 and OH were used as oxidants in the controlled conditions in these experiments. Our motivation is to evaluate the roles that these oxidants play in the formation of new particles and in the subsequent condensational growth. We also determine aerosol chemical compositions and densities. By using actual pine seedlings as source of VOCs, we are able to get realistic and important information on what process are dominant in atmospheric aerosol formation.

2 Experimental description

The major components of the experimental system consisted of a biogenic emission enclosure, reaction chamber and both gas phase and aerosol particle sampling systems. A block diagram of this system is shown in Fig. 1 and the overall system components and analysis methods will be described in detail below.

2.1 Plant materials

Scots pine seedlings (1 year-old) were obtained from a forest nursery (Finnish Forest Research Institute, Suonenjoki Research Unit, Suonenjoki, Finland) in May and planted in 7.5 l plastic pots in 2:1 (*v/v*) quartz sand (Ø 0.5–1.2 mm, SP Minerals Partek, Finland) and fertilized sphagnum peat (Kekkilä PP6, Finland). After planting, seedlings were growing in the open field site (Research Garden, University of Kuopio) until the end of July. Then the seedlings were taken in a greenhouse to avoid onset of winter dormancy. In October, prior to the experiments, the seedlings were kept in growth chambers (see Vuorinen et al., 2004 for more detail) in temperature conditions of +22°C. To simulate herbivore attack on tree bark and to activate the chemical defense of seedlings, 3 cm long and 2 mm deep cuts were made on the base of main stem by a knife. After these preparations, two seedlings were selected as the trial plants and placed carefully in two individual transparent Neoflon™ FEP bags. These bags served as manifolds through which air passed in and out of the enclosure to take the pine emissions. Six lamps (Lival Shuttle Plus, Lival Oy, Sipoo, Finland, 24W, PAR ca. 350 µmol m^{-2} s^{-1}) were utilized to ensure the optimal photosynthesis activity and VOC emissions.

2.2 Reaction chamber experiments

The reaction chamber for this study is a 6 m^3 rectangular chamber made of Neoflon™ FEP film, which is attached to a stainless steel frame. The height of the chamber is 2.5 m with the bottom area of 1.0×2.4 m^2. Prior to every experiment, the chamber was continuously flushed by laboratory compressed clean air for overnight. The compressed air was processed through activated charcoal, Purafil™ select and absolute HEPA filter, to get rid of hydrocarbons, NO_x and particles.

Prior to experiments, clean air flow took the pine emissions into the chamber through Teflon lines until the desired concentration of terpenes was achieved. In some experiments, tetramethylethylene (TME) (99+%, Aldrich) was delivered into the chamber via sending air through a heated bulb containing a known volume of TME and into the

chamber. TME was used to produce hydroxyl radical (OH) radical. It was chosen because TME ozonolysis requires neither NO_x nor UV photolysis, and it can result in an OH yield near unity (Lambe et al., 2007; Paulson et al., 1997). In one group of the experiments, 2-butanol, used as OH scavenger, was introduced into the chamber in a similar manner as TME. The concentration of 2-butanol injected was approximately 600-fold higher than terpenes so that the reaction rate of OH with scavenger exceeded that of OH with parent hydrocarbons by a factor of 100 (Keywood et al., 2004; Docherty et al., 2003; Ziemann et al., 2003). Major products of OH-2-butanol reaction are 2-butanone (with yield of 69% at room temperature) and acetone (with yield range from 12–29%) (Aschmann et al., 2002; Jiménez et al., 2005), which have high vapor pressures suggesting that they are too volatile to partition into the particle phase. After injections of above reactants, ozone was generated by a UV lamp O_3 generator. The air flow (40 L min^{-1}) enriched with ozone (60–800 ppb) at the inlet of the chamber was added. Ozone and TME were kept separated until inside the chamber because of the short lifetime of OH radical. The beginning of first ozone injection marks the start of each experiment. In all experiments, temperature was controlled in the range of 25±2°C and relative humidity (RH) in 35±5%. No seed aerosols were added and the chamber was kept dark with a black polyethylene covering.

2.3 Analysis methods and instrumentation

Nitric oxide (NO), total NO_x and SO_2 concentration inside the chamber were measured with an AC 30M NO_x analyzer and AF21M SO_2 analyzer (Environment s.a.), respectively. O_3 concentration was monitored at the inlet and inside the chamber by two DASIBI 1008-RS O_3 analyzers (Dasibi Environmental Corporation, Glendele, CA, USA). Temperature and RH were measured continuously using a RH and temperature transmitter (Vaisala Humitter Y50). In all the experiments, SO_2 concentration was lower than the detectable limit of analyzer (~1 ppb). The low level of SO_2 concentration would make the potential influence of H_2SO_4 on the new particle nucleation to be negligible.

VOC emissions from pine seedlings were measured using two instruments, a gas

CC BY

chromatography-mass spectrometer (GC-MS, Hewlett-Packard GC model 6890, MSD 5973) for off-line analysis and a proton transfer reaction mass spectrometer (PTR-MS, Ionicon Analytik GmbH) for on-line analysis. VOCs were sampled on about 150 mg *Tenax TA* adsorbent (Supelco, mesh 60/80) for 15 or 30 min.Then the collected VOCs were analyzed with GC-MS run by temperature-controlled analysis program. Identification of the compounds was based on the molecular retention time and comparison of mass spectra with those of pure standards. The analysis method used here has been described in detail elsewhere (Pinto et al., 2007; Joutsensaari et al., 2005; Vuorinen et al., 2004). PTR-MS was used to monitor concentrations of selected parent hydrocarbons and various gas-phase intermediates and products continuously over the course of experiments. A detailed description of PTR-MS technique is given by Lindinger et al. (1998) and De Gouw and Warneke (2007). The calibration procedure and mixing ratio calculations were described in Taipale et al. (2008). During every experiment full scan mode was used to see if there were important compounds other than the selected ones that were measured continuously. Ions were monitored with mass-to-charge (m/z) consistent with formaldehyde (m/z=30+1), methanol (32+1), acetone (m/z=58+1), isoprene (m/z=68+1), TME (m/z=84+1), monoterpenes (m/z=136+1) and sesquiterpenes (m/z=204+1).

Aerosol chemical composition and mass size distributions were measured by an Aerodyne Aerosol Mass Spectrometer (AMS). Detailed descriptions of the AMS measurements principles and various calibrations, its operation mode and data processing methods can be found in other publications (Jayne et al., 2000; Allan et al., 2003, 2004; Jimenze et al., 2003a, 2003b; Zhang et al., 2004). Briefly, the AMS uses an aerodynamic lens to focus particles into a tight beam that is introduced into a high vacuum tube (10^{-8} Torr). Particles are detected as they impact on a porous tungsten surface which is heated typically to 600°C.The volatile and semi-volatile fractions of the aerosols are vaporized and immediately ionized by a 70 eV electron source. The resulting positive ion fragments are detected by a Quadrupole Mass Spectrometer (QMA 430, Balzers Instruments, Balzers, Liechtenstein). Particle size is calculated from the

CC BY

particle flight of time. MS spectrum is achieved by the difference of background signal and total signal.

Aerosol particle size distributions over a ranger of 5.6–560 nm were measured using a fast mobility particle sizer spectrometer (FMPS, TSI model 3091). FMPS was operated with aerosol and sheath flows of 10 and 40 $L min^{-1}$. The high measurement resolution (sampling in 1 s resolution and averaged in 5 min resolution in this study) enables us to visualize particle size distributions during nucleation events.

2.4 Effective density

AMS measures the vacuum aerodynamic diameter (D_{va}), defined as the diameter of a standard density (ρ_0) sphere with the same terminal velocity as the interested particle in a free-molecular regime. FMPS instead provides a measurement of the mobility diameter (D_m), known as the diameter of a sphere with the identical migration velocity of particle in a constant electric field in the atmospheric pressure. The effective density of particle, ρ_{eff}, is simply defined as ratio of the vacuum aerodynamic and mobility diameter multiplied by unit density (Jimenez et al., 2003b; DeCarlo et al., 2004; Bahreini et al., 2005).

$$\rho_{\text{eff}} = \rho_0 \frac{D_{va}}{D_m} = \rho_p \frac{D_{ve}}{X_{ve} D_m} \tag{1}$$

where ρ_p is the material density and ρ_0 is the unit density (1 g cm^{-3}). D_{ve} is the diameter of a spherical particle having the same volume as the particle under consideration. X_{ve} is the dynamic shape factor in the free-molecular regime.

For spherical particles, the effective density is equivalent to the particle density, while the effective density can be significantly different for particle with an irregular shape. Note that various definitions of effective density are used in the literature. These definitions do not yield the same numerical values for irregular particles (DeCarlo et al., 2004). In this study, a series of mobility diameters measured by FMPS was compared

CC BY

to their corresponding vacuum aerodynamic diameters measured by AMS in parallel in order to determine the densities of SOA particles.

2.5 Modeling of VOC oxidation

Since new particle formation is initiated by the gas-phase oxidation of VOCs, a kinetic model of VOCs from the oxidation of O_3 and OH was built to interpret the new particle nucleation and growth events. In this model, the oxidation of VOCs was calculated using the initial measured concentrations of VOCs and known reaction rates. O_3 and OH are assumed to be involved in the oxidation reactions of VOCs and TME, taking into account the secondary loss process of OH and O_3. In brief, O_3 and OH initiated oxidation of these VOCs produce condensing and nucleating species, OH radicals and other volatile compounds.

$$\mathrm{VOC}_i + \mathrm{O_3} \xrightarrow{k_{\mathrm{O_3}}^{\mathrm{VOC}_i}} \mathrm{OH\ radical + volatile + semivolatile + nonvolatile\ species}\,, \quad (2)$$

$$\mathrm{VOC}_i + \mathrm{OH} \xrightarrow{k_{\mathrm{OH}}^{\mathrm{VOC}_i}} \mathrm{volatile + semivolatile + nonvolatile\ species}\,. \quad (3)$$

Once TME is added into the experimental systems, ozonolysis of TME leads to the production of OH radical

$$\mathrm{TME} + \mathrm{O_3} \xrightarrow{k_{\mathrm{O_3}}^{\mathrm{TME}}} \mathrm{OH + other\ products}\,. \quad (4)$$

So, the formation rate of OH radical ($f\mathrm{OH}$) can be calculated using the following equitation

$$f\mathrm{OH} = \omega_i k_{\mathrm{O_3}}^{\mathrm{TME}}[\mathrm{TME}][\mathrm{O_3}] + \sum_i \omega_i' k_{\mathrm{O_3}}^{\mathrm{VOC}_i}[\mathrm{VOC}]_i[\mathrm{O_3}]\,, \quad (5)$$

where ω_i, ω_i' denote the yields of hydroxyl radicals from the O_3 reactions, and k is reaction constants of the chemical reactions.

Thus there is a competition in reactions of O_3 with TME and monoterpenes during the initial stage of reaction. The average consumption rate of O_3 can be expressed as

$$\frac{d[O_3]}{dt} = \frac{d[O_3]_{inlet}}{dt} - \gamma_i k_{O_3}^{TME}[TME][O_3] - \sum_i \gamma_i' k_{O_3}^{VOC_i}[VOC]_i[O_3] , \quad (6)$$

where γ_i and γ_i' are the correction factors to take into account the secondary loss of ozone with the second-generation products. These correction factors were estimated according to the VOC molecular structures and the complexities of their reactions with O_3 and OH and further confirmed by a model sensitivity test.

Due to the high reaction rate of OH+TME, the added TME also resulted in OH loss

$$TME + OH \xrightarrow{k_{OH}^{TME}} products . \quad (7)$$

Reactions (2–5,7) give the time-dependent OH concentration as

$$\frac{d[OH]}{dt} = fOH - \gamma_i'' k_{OH}^{TME}[TME][OH] - \sum_i \gamma_i''' k_{OH}^{VOC_i}[VOC]_i[OH] , \quad (8)$$

where γ_i'' and γ_i''' are the correction factors to take into account the secondary loss of OH with the second-generation products. All the parameters used in the model are listed in Table 1.

Products from the O_3- plus OH-initiated TME oxidation are formaldehyde, methanol and acetone and some minor compounds (Niki et al., 1987; Tuazon et al., 1997; Tuazon et al., 1998). The vapor pressures of these species are too high to take part into aerosol nucleation and growth processes and so are omitted from the model. Berndt et al. (2004) have also shown that ozonolysis of TME in the absence of SO_2 leads to no observable new particle formation. Thus, in this paper, O_3 and OH oxidation rates (excluding the contributions from TME) with VOCs are defined as

$$r_{O_3} = \sum_i k_{O_3}^{VOC_i}[VOC]_i[O_3] , \quad (9)$$

CC BY

$$r_{OH} = \sum_i k_{OH}^{VOC_i}[VOC]_i[OH] \,. \quad (10)$$

New particle formation rate (F) and growth rate (G) can be constrained directly by the oxidation rates of VOCs

$$F \sim r_{O_3} + r_{OH} \,, \quad (11)$$

$$G \sim r_{O_3} + r_{OH} \,. \quad (12)$$

Similarly, for the loss of other compounds and formation of products, chemical kinetics can be described using the following rate equations

$$\frac{d[VOC]_i}{dt} = -\sum_i k_{O_3}^{VOC_i}[VOC]_i[O_3] - \sum_i k_{OH}^{VOC_i}[VOC]_i[OH] \,, \quad (13)$$

$$\frac{d[TME]}{dt} = -k_{O_3}^{TME}[TME][O_3] - k_{OH}^{TME}[TME][OH] \,, \quad (14)$$

$$\frac{d[AT]}{dt} = \sum_i \beta_i k_{O_3}^{VOC_i}[VOC]_i[O_3] + \sum_i \beta_i' k_{OH}^{VOC_i}[VOC]_i[OH] - k_{OH}^{AT}[AT][OH] \,, \quad (15)$$

$$\frac{d[FAH]}{dt} = \sum_i \alpha_i k_{O_3}^{VOC_i}[VOC]_i[O_3] + \sum_i \alpha_i' k_{OH}^{VOC_i}[VOC]_i[OH] - k_{OH}^{FAH}[FAH][OH] \,, \quad (16)$$

where β_i, β_i' are the yields of acetone (AT) from reactions of O_3 and OH with VOCs and TME and α_i, α_i' are for the formaldehyde (FAH) yield.

2.6 Summary of experiments performed

Five experiments were carried out in the present study. The initial conditions are summarized in Table 2. TME was added in E1a–E1c to investigate the role of OH-initiated oxidation in new particle formation. No TME was added in E2 in order to simulate lower OH conditions. Experiment E3 was performed in the presence OH scavenger to investigate the role of ozonolysis alone in new particle formation.

3 Results and discussion

3.1 Scots pine emissions

The emitted VOCs from the Scots pine seedlings included monoterpenes, isoprene and minor amounts of other small molecular compounds, e.g. methanol, with monoterepenes dominating the total emissions in this work. Monoterpenes included α-pinene, β-pinene, Δ^3-carene, β-phellandrene, limonene and myrcene, making up more than 95% of the total VOC emissions as tabulated in Table 3. In E1c and E3, there was no detectable Δ^3-carene and very high contribution of β-pinene to total VOC emissions was observed in E1c. The variability in contributions of emission species in every case, specially dominated by α-pinene, limonene and Δ^3-carene, might be due to the emission rates of monoterpenes that were sensitive to the ambient environmental conditions (Räisänen et al., 2008; Tarvainen et al., 2005), but also strongly dependent on the frequency of Δ^3-carene-rich genotype (Manninen et al., 1998). Field results in Finnish forest have demonstrated the dependence of monoterpene emission rates on environmental temperature and light intensity (Räisänen et al., 2008; Tarvainen et al., 2005). In all cases, sesquiterpenes in the emitted compounds were lower than 0.05 ppb as determined with PTR-MS measurements. This is consistent with observations in Hyytiällä forest of Finland that sesquiterpene emissions from Scots pine are only 2–5% of the total monoterpene emission rates and emission, with emissions ceasing in September (Tarvainen et al., 2005).

According to the measurements made in two locations in Finland, the major emitted compounds from Scots pine are α-pinene, β-pinene and Δ^3-carene, with approximate contributions of 60–85% to the total observed monoterpene emission rates, although late in the autumns β-phellandrene can make 20% of total monoterpene emission (Räisänen et al., 2008). Lindfors and Laurila (2000) estimated that total biogenic VOC emissions from Finnish forest are dominated by monoterpenes, which contribute approximately 45%, while in deciduous trees percentage can be as low as 10–15% (Mäntylä et al., 2008), and isoprene emission are only 7% of annual total. In the

ACPD
9, 8223–8260, 2009

US the main biogenic monoterpene emissions are α-pinene, β-pinene, and limonene (Sakulyanontvittaya et al., 2008). Thus the emission spectrum in this study is very consistent with natural Scots pine and the monoterpene distributions in Europe and USA, making this work more representative of the atmospheric reaction conditions than pure VOCs or mixtures of pure VOCs commonly used in chamber experiments.

3.2 Formation of new particles

3.2.1 Reaction of emitted VOCs

Figure 2 shows the decay profiles of ten kinds of VOCs as tabulated in Table 3 (panel A) and formation curves of gas-phase product of acetone and formaldehyde as functions of time (panel B) in experiment E1a. The modelled concentrations were calculated based on the OH and O_3 induced chemistry of these VOCs as described in Sect. 2.5. Possbile formation sources of acetone and formaldehyde include O_3 and OH induced chemisty of TME and emitted VOCs as shown in Eqs. (15) and (16). Degraded products of these ten VOCs will contribute to new particle formation and will be described in following sections. Good agreement between modelled and modeled VOC and product concentrations provides further confirmation to the validity of the model used in this study.

3.2.2 New particle from OH+O_3 induced chemistry

As the emissions of pine seedlings were oxidized by O_3 and OH, various products of different volatility were formed. Homogeneous nucleation occurs when the non-volatile products exceeded their saturation vapor pressure sufficiently. Later on, the semi-volatile species begin condensing on the surface of the pre-formed particle, causing an increase in particle size and aerosol volume concentration. The contour plots of aerosol particle number size distributions, total number/volume concentrations and gas-phase species concentration are illustrated in Fig. 3. In these systems, OH radi-

cals are produced not only in the course of ozonolysis of TME but also in the ozonolysis of monoterpenes. Both the OH- and O_3-initiated oxidation of monoterpenes might contribute to the new particle formation. At high concentration of TME, ozonolysis of TME was expected to produce high amount of OH radicals based on Eq. (4). It can be seen that a rapid increase in the particle number concentration occurred and obvious nucleation events took place after the first addition of ozone in all cases. However, the maximum number concentration was 27 700 particle cm^{-3} in the highest TME experiment (E1c), which was much lower than the 128 000 particle cm^{-3} in the lowest TME case (E1a). In experiments with two ozone additions, the second ozone injection induced very weak increase of aerosol number concentrations, but an intensive increase in aerosol volume concentrations.

3.2.3 New particles from ozonolysis reaction

In experiment E3, 2-butanol was added into the chamber to remove the OH in the gas phase. 2-butanol is known to scavenge efficiently the OH radicals and our goal was to ensure that only ozonolysis reactions occur in the system. Figure 4 shows the particle profiles of the ozonolysis experiments. Only a very weak nucleation event was observed in this experiment. The maximum number concentration was only 8120 particle cm^{-3}, being much lower than that was found during OH/O_3 initiated cases. On the other hand, a relatively high increase rate in aerosol volume was observed.

3.2.4 Nucleation and growth rates

The experiments described here emphasize the variability in new particle formation from initiation by different oxidation sources. The roles of OH- and O_3- induced oxidation in the new particle formation can be interpreted using the chemistry model results. The correlations of instantaneous nucleation and condensational growth rates with the oxidation reaction rates of monoterpenes with OH and O_3 are shown in Fig. 5. Nucleation events usually ended at the initial stages of reaction in this study (less

CC BY

than 60 min after the beginning of experiment) and growth continued as long as there was VOCs and O_3 available. In E1a, very fast aerosol nucleation, with rate as high as 360 $cm^{-3}\,s^{-1}$, was observed, consistent with the rapid OH oxidation rates calculated with the model. And in the pure ozonolysis experiment (E3, with OH scavenger present), nucleation rate was very low (<0.5 $cm^{-3}\,s^{-1}$), despite the very fast O_3 oxidation rate. These results indicate that OH-initiated oxidation reactions play a very important role in the aerosol nucleation stages and ozonolysis of monoterpenes are less effectively involved in the aerosol nucleation process under these experimental conditions.

As can be seen from Fig. 5, the modeled OH and O_3 reaction rates also show good correlations with the condensational growth rates in E1–E3 experiments, suggesting that OH and O_3 reactions both play roles in particle growth process. Furthermore, in E3, the highest aerosol growth rate of 74 $nm\,h^{-1}$ was achieved where the OH reaction rate was slow, suggesting that the ozonolysis of VOCs is more efficient for aerosol growth.

Nucleation rates were found to be lower even under cases of high OH reaction rates (e.g. E1c and E2). It might be due to the emission spectrum distributions in each experiment. The nucleation potential of one biogenic compound depends on the combination of its abundance and its efficiency for nucleation. VanReken et al. (2006) reported that the presence of β-pinene probably inhibited particle formation in the Holm oak (*Quercus ilex*) experiment. The high contributions of β-pinene to the total VOC mix might thus lead to the lower nucleation rate in E1c.

Nucleation and growth from the oxidation of monoterpenes by OH and O_3 has been studied over the past ten years (Bonn and Moortgat, 2002; Burkholder et al., 2007; Hoppel et al., 2001; Griffin et al., 1999; Mentel et al., 2009). Most studies were performed using one monoterpene such as α-pinene and β-pinene as representative compounds to assess the OH and O_3 initiated oxidation on the new particle formation efficiency. Bonn and Moortgat used a scanning mobility particle sizer (SMPS) to study the new particle formation during the oxidation of α- and β-pinene by O_3 and OH in

CC BY

a 0.57 m^3 spherical glass vessel. By comparisons of the aerosol number and volume concentrations in different cases, they reported that ozonolysis of monoterpenes was much more efficient for nucleation than what was the observed for OH-initiated case. This contradicts our results in which ozonolysis is less effective in nucleation process. Our results are consistent with the results of Burkholder et al. (2007), which find that monoterpene ozonolysis alone (with no OH radical reaction) cannot yield significant particle formation. However, ozonolysis does contribute to particle growth. The results of this study are strong agreement with recent work showing that for the oxidation of pine emissions, ozonolysis does not induce particle formation and OH radicals are essential for the new particle formation (Mentel et al., 2009).

3.3 Chemical signatures

Chemical signatures of the newly formed aerosols during the above experiments were investigated utilizing the AMS. Figure 6 displays the average mass spectra of SOA for the first hour and second hour for each experiment. All spectra were normalized to total mass signal. We can see that most of the spectra were characterized by some intense mass fragments at *m/z* 27, 29, 41, 43, 44, 51, 55, 65, 77 and 141. Mass Fragments 27, 29, 41, 43 and 55 represented the ion series of $C_nH^+_{2n-1}$ and $C_nH^+_{2n+1}$ and separated by 14 mass units due to loss of CH_2, which can indicate the presence of heavily saturated and non-oxidized hydrocarbon-like organic species (Alfarra et al., 2006; Allan et al., 2006). Another potential contribution to mass 43 is an oxygen-containing fragment, CH_3CO^+. Fragment 44 corresponds to CO_2^+, which represents highly oxidized classes of compounds containing carbonyl and carboxylic acid functional groups (Alfarra et al., 2006). Peaks at mass 51, 77 and 141 may be from the ozonolysis reaction of VOCs but their identifications are unclear at present.

In the TME experiments (E1b and E1c), mass spectra were dominated by mass fragment 44, contributing to as high as 20.5% and 13.8% to the total first hour mass signal, respectively. As a comparison, during OH-scavenged experiment (Left panel E3 in

CC BY

Fig. 6), no fractional contribution by *m/z* 44 signals was found in the first hour. This indicates OH plays a key role in forming species which fragment to give *m/z* 44 species. The importance of OH reaction for each VOC (as a percentage of total reaction) during new particle formation is presented in Table 4. Values were calculated from the following equation:

$$\text{fraction} = \frac{\int_0^t r_{i,\mathrm{OH}(t)}\mathrm{d}t}{\int_0^t r_{i,\mathrm{OH}(t)}\mathrm{d}t + \int_0^t r_{i,\mathrm{O_3}(t)}\mathrm{d}t}, \quad (17)$$

where $r_{i,\mathrm{OH}(t)}$ and $r_{i,\mathrm{O_3}(t)}$ were the reaction rates of VOC_i with OH and $\mathrm{O_3}$ at time t (min), respectively.

In all the OH-dominated experiments (E1a–1c), all VOCs but terpinolene reacted primarily (>75%) with OH rather than $\mathrm{O_3}$. For E2, both $\mathrm{O_3}$- and OH-initiated oxidation were important, with the fraction of OH reaction varying from 8.4% (terpinolene) to 97.8% (myrcene). And in ozonolysis case (E3), ozonolysis dominated for all VOCs except camphene. The relative importance of OH reactions in all experiments corresponds well to the mass fraction of *m/z* 44 ions, strongly suggesting that OH-initiated oxidation leads to the formation of highly oxidized aerosol species. On the other hand, the very high contribution of *m/z* 43 signal to the mass loadings in E3 suggests that ozonolysis reaction might contribute more to the less oxidized products.

Averaged mass spectra appeared to have highly similar fragmentation patterns during the second hour, implying the products formed have broadly similar chemical functionality in these experiments. These similarities in the mass spectra were further confirmed in longer reaction time (not shown in Fig. 6), suggesting that once particles were formed, the chemical signature detected by AMS did no change significantly under these experimental conditions. However, significant difference for the minor mass fragments occurred, suggesting that the SOA particles might have different chemical compositions.

The mass spectra measured in the present studies also share some common features with those measured in the real atmosphere. The mass spectrum from particles

following a nucleation event exhibited the signals at *m/z* 27, 29, 41, 43, 44, 51, 55, 57, 77, 91 and 141 (Alfarra et al., 2006; Allan et al., 2006; Salcedo et al., 2006). The similarities in our measurements and the ambient mass spectra indicate that the experimental results are able to reproduce the products distributions of SOA formed in the real atmosphere.

3.4 Effective density (ED)

Effective density of SOA particle was calculated followed the approach outlined in Sect. 2.4. In this method, the mobility and vacuum aerodynamic diameters were identified from the peak values by using a log-normal fitting to volume/mass size distributions. Table 5 lists parts of selected particle mobility diameters, the measured aerodynamic diameters and the corresponding effective density after the initial growth of particles.

The determined effective density from the OH and O_3 oxidation induced SOA was $1.34\pm0.06\,g\,cm^{-3}$, nearly identical to the value of $1.38\pm0.03\,g\,cm^{-3}$ of particles from the ozonolysis reaction systems. The results show that the effective density for both types of SOA is not substantially impacted by the initiating oxidants. The density is also found to be independent of the particle size within the accumulation mode. However the effective density showed a dependence on the particle size with Aitken mode in this work and these results need further confirmation. Our reported aerosol densities are in agreement with measured densities of $1.25\pm0.15\,g\,cm^{-3}$ of SOAs from real pine emissions (Mentel et al., 2009). These results are also consistent with density measurements of $1.2–1.7\,g\,cm^{-3}$ for ambient aerosol and laboratory-generated monoterpene SOA (Shilling et al., 2009; Saathoff et al., 2008; Bahreini et al., 2005; Alfarra et al., 2006; Kostenidou et al., 2007; Kannosto et al., 2008).

Accurate measurements of density are very important to convert the aerosol volume concentration to mass loadings. The effective density is heavily affected by the material real density and particle shape factor (Bahreini et al., 2005; DeCarlo et al., 2004). Alfarra et al. (2006) reported shape of SOA formed from the photooxidation of α-pinene

CC BY

to be spherical. In their experiments, effective densities were equivalent to the material densities. However, SOA particles are reported to be in solid or waxy phase with densities larger 1.25 g cm^{-3} from the ozonolysis of biogenic emissions (Kostenidou et al., 2007). Irregular shapes of the solid or waxy aerosol make the effective density lower than the real material density. In this study, our aerosol might be in nonspherical shapes and our ongoing biogenic SOA experiments are investigating this possibility. This will be further discussed in future work.

4 Conclusions

We have studied freshly formed aerosols following the gas phase oxidation of the direct emissions of Scots pine (*Pinus sylvestris L.*) seedlings in a smog chamber. New particle formation following the ozonolysis and O_3 plus OH initiated oxidation was measured. 2-butanol and TME were used to control the ratios of O_3 and OH concentrations. Emitted species, aerosol nucleation and condensational growth events, chemical compositions and density of the new formed particles are measured and investigated in this study.

Major emitted VOCs from Scot pine included monoterpenes and isoprene. Ozone plus OH initiated oxidation of these VOCs produced large amounts of new particles. For new aerosol formation, OH-initiated oxidation plays a critical role in a nucleation during the initial stage of new particle formation. Ozonolysis seems to be more efficiently involved in the particle condensational growth, but it does not contribute substantially to nucleation. These results demonstrate that OH oxidation of VOCs could be a source of the new organic particles in the atmosphere.

Mass spectral results show that highly oxidized compounds (*m/z* 44 signals) contribute more to SOA formed from OH radical initiated oxidation of emitted VOCs during the initial stage of nucleation events. Ozonolysis of emitted VOCs produces SOA which is less oxidized with the mass spectrum dominated by the *m/z* 43 ions. In a long run, the mass spectral patterns in different experiments do not change significantly, indicat-

ACPD
9, 8223–8260, 2009

ing the SOA produced have broadly similar chemical functionality.

From AMS and FMPS data it was determined that the aerosol effective densities are almost identical in these two oxidation systems, implying that the products formed by the different oxidants have roughly similar densities.

The experiments carried out here were designed to match atmospheric conditions as closely as possible, so that the present results may be applicable to new particle formation and growth in the atmosphere, particularly in pristine forested environments. The oxidants (O_3 and OH) and organics (monoterpenes) studied are among the most important in the troposphere; concentrations of OH and monoterpenes approached tropospheric levels; and the organics included an atmospherically relevant mixture of monoterpenes (direct vegetation emissions).

Acknowledgements. This work was funded by the Academy of Finland (decision no. 120802, 111543, 123466 and Centre of Excellence Programme). We thank the staff at the Kuopio University Research Garden for maintaining the plants.

References

Alfarra, M. R., Paulsen, D., Gysel, M., Garforth, A. A., Dommen, J., Prévôt, A. S. H., Worsnop, D. R., Baltensperger, U., and Coe, H.: A mass spectrometric study of secondary organic aerosols formed from the photooxidation of anthropogenic and biogenic precursors in a reaction chamber, Atmos. Chem. Phys., 6, 5279–5293, 2006, http://www.atmos-chem-phys.net/6/5279/2006/.

Allan, J. D., Alfarra, M. R., Bower, K. N., Coe, H., Jayne, J. T., Worsnop, D. R., Aalto, P. P., Kulmala, M., Hyötyläinen, T., Cavalli, F., and Laaksonen, A.: Size and composition measurements of background aerosol and new particle growth in a Finnish forest during QUEST 2 using an Aerodyne Aerosol Mass Spectrometer, Atmos. Chem. Phys., 6, 315–327, 2006, http://www.atmos-chem-phys.net/6/315/2006/.

Allan, J. D., Delia, A. E., Coe, H., Bower, K. N., Alfarra, M. R., Jimenez, J. L., Middlebrook, A. M., Drewnick, F., Onasch, T. B., Canagaratna, M. R., Jayne, J. T., and Worsnop, D. R.:

A generated method for the extraction of chemically resolved mass spectra from aerodyne aerosol mass spectrometer data, J. Aerosol Sci., 35, 902–922, 2004.
Allan, J. D., Jimenez, J. L., Williams, P. I., Alfarra, M. R., Bower, K. N., Jayne, J. T., Coe, H., and Worsnop, D. R.: Quantitative sampling using an aerodyne aerosol mass spectrometer 1. Techniques of data interpretation and error analysis, J. Geophys. Res., 108, 4090, doi:10.1029/2002JD002358, 2003.
Aschmann, S. M., Arey, J., and Atkinson, R.: OH radical formation from the gas-phase reactions of O_3 with a series of terpenes, Atmos. Environ., 36, 4347–4355, 2002.
Atkinson, R. and Arey, J.: Atmospheric degradation of volatile organic compounds, Chem. Rev., 103, 4605–4638, 2003a.
Atkinson, R. and Arey, J.: Gas-phase tropospheric chemistry of biogenic volatile organic compounds: a review, Atmos. Environ., 37, S197–S219, 2003b.
Bahreini, R., Keywood, M. D., Ng, N. L., Varutbangkul, V., Gao, S., Flagan, R. C., Seinfeld, J. H., Worsnop, D. R., and Jimenez, J. L.: Measurements of secondary organic aerosol from oxidation cycloalkenes, terpenes, and m-Xylene using an aerodyne aerosol mass spectrometer, Environ. Sci. Technol., 39, 5674–5688, 2005.
Berndt, T., Böge, O., and Stratmann, F.: Atmospheric particle formation from the ozonolysis of alkenes in the presence of SO_2, Atmos. Environ., 38, 2145–2153, 2004.
Bonn, B. and Moortgat, G. T.: New particle formation during α- and β-pinene oxidation by O_3, OH and NO_3, and the influence of water vapour: particle size distribution studies, Atmos. Chem. Phys., 2, 183–196, 2002, http://www.atmos-chem-phys.net/2/183/2002/.
Burkholder, J. B., Baynard, T., Ravishankara, A. R., and Lovejoy, E. R.: Particle nucleation following the O_3 and OH initiated oxidation of α-pinene and β-pinene between 278 and 320 K, J. Geophys. Res., 112, D10216, doi:10.1029/2006JD007783, 2007.
Claeys, M., Graham, B., Vas, G., Wang, W., Vermeylen, R., Pashynska, V., Cafmeyer, J., Guyon, P.,Andreae, M. O., Artaxo, P., and Maenhaut, W.: Formation of secondary organic aerosols through photooxidation of isoprene, Science, 303, 1173–1176, 2004.
DeCarlo, P. F., Slowik, J. G., Worsnop, D. R., Davidovits, P., and Jimenez, J. L.: Particle morphology and density characterization by combined mobility and aerodynamic diameter measurements. Part 1: Theory, Aerosol Sci. Technol., 38, 1185–1205, 2004.
de Gouw, J. and Warneke, C.: Measurements of volatile organic compounds in the earths atmosphere using proton-transfer-reaction mass spectrometry, Mass Spec. Rev., 26, 223–

257, 2007.
Docherty, K. S. and Ziemann, P. J.: Effects of stabilized Criegee intermediate and OH radical scavengers on aerosol formation from reactions of β-Pinene with O_3, Aerosol Sci. Technol., 37, 877–891, 2003.
Gao, S., Keywood, M., Ng, N. L., Surratt, J., Varutbangkul, V., Bahreini, R., Flagan, R. C., and Seinfeld, J. H.: Low-molecular-weight and oligomeric components in secondary organic aerosol from the ozonolysis of cycloalkenes and α-Pinene, J. Phys. Chem. A., 108, 10147–10164, 2004.
Guenther, A., Hewitt, C. N., Erickson, D., Fall, R., Geron, C., Graedel, T., Harley, P., Klinger, L., Lerdau, M., Mckay, W. A., Pierce, T., Scholes, B., Steinbrecher, R., Tallamraju, R., Taylor, J., and Zimmerman, P.: A global-model of natural volatile organic-compound emissions, J. Geophys. Res., 100, 8873–8892, 1995.
Griffin, R. J., Cocker III, D. R., Flagan, R. C., and Seinfeld, J. H.: Organic aerosol formation from the oxidation of biogenic hydrocarbons, J. Geophys. Res., 104, 3555–3567, 1999.
Grosjean, E., DeAndrade, J. B., and Grosjean, D.: Carbonyl products of the gas-phase reaction of ozone with simple alkenes, Environ. Sci. Technol., 30, 975–983, 1996.
Hoffmann, T., Odum, J. R., Bowman, F., Collins, D., Klockow, D., Flagan, R., and Seinfeld, J. H.: Formation of organic aerosols from the oxidation of biogenic hydrocarbons, J. Atmos. Chem., 26, 189–222, 1997.
Hoppel, W., Fitzgerald, J., Frick, G., Caffrey, P., Pasternack, L., Hegg, D., Gao, S., Leaitch, R., Shantz, N., Cantrell, C., Albrechcinski, T., Ambrusko, J., and Sullivan, W.: Particle formation and growth from ozonolysis of a-pinene, J. Geophy. Res., 106, 27603–27618, 2001.
Jayne, J. T., Leard, D. C., Zhang, X. F., Davidovits, P., Smith, K. A., Kolb, C. E., and Worsnop, D. R.: Development of an aerosol mass spectrometer for size and composition analysis of submicron particles, Aerosol Sci. Technol., 33, 49–70, 2000.
Jang, M. and Kamens, R. M.: Newly characterized products and composition of secondary aerosols from the reaction of alpha-pinene with ozone, Atmos. Environ., 33, 459–474, 1999.
Jiménez, E., Lanza, B., Garzón, A., Ballesteros, B., and Albaladejo, J.: Atmospheric degradation of 2-Butanol, 2-Methyl-2-butanol, and 2,3-Dimethyl-2-butanol: OH kinetics and UV absorption cross sections, J. Phys. Chem. A., 109, 10903–10909, 2005.
Jimenez, J. L., Jayne, J. T., Shi, Q., Kolb, C. E., Worsnop, D. R., Yourshaw, I., Seinfeld, J. H., Flagan, R. C., Zhang, X. F., Smith, K. A., Morris, J. W., and Davidovits P.: Ambient aerosol sampling using the aerodyne aerosol mass spectrometer, J. Geophys. Res., 108, 8425,

doi:10.1029/2001JD001213, 2003a.
Jimenez, J. L., Bahreini, R., Cocker III, D. R., Zhuang, H., Varutbangkul, V., Flagan, R. C., Seinfeld, J. H., O'Dowd, C. D., and Hoffmann, T.: New particle formation from photooxidation of diiodomethane (CH_2I_2), J. Geophys. Res., 108, 4318, doi:10.1029/2002JD002452, 2003b.
Joutsensaari, J., Loivämaki, M., Vuorinen, T., Miettinen, P., Nerg, A.-M., Holopainen, J. K., and Laaksonen, A.: Nanoparticle formation by ozonolysis of inducible plant volatiles, Atmos. Chem. Phys., 5, 1489–1495, 2005, http://www.atmos-chem-phys.net/5/1489/2005/.
Kanakidou, M., Seinfeld, J. H., Pandis, S. N., Barnes, I., Dentener, F. J., Facchini, M. C., Van Dingenen, R., Ervens, B., Nenes, A., Nielsen, C. J., Swietlicki, E., Putaud, J. P., Balkanski, Y., Fuzzi, S., Horth, J., Moortgat, G. K., Winterhalter, R., Myhre, C. E. L., Tsigaridis, K., Vignati, E., Stephanou, E. G., and Wilson, J.: Organic aerosol and global climate modelling: a review, Atmos. Chem. Phys., 5, 1053–1123, 2005
Kannosto, J., Virtanen, A., Lemmetty, M., Mäkelä, J. M., Keskinen, J., Junninen, H., Hussein, T., Aalto, P., and Kulmala, M.: Mode resolved density of atmospheric aerosol particles, Atmos. Chem. Phys., 8, 5327–5337, 2008, http://www.atmos-chem-phys.net/8/5327/2008/.
Keywood, M. D., Kroll, J. H., Varutbangkul, V., Bahreini, R., Flagan, R. C., and Seinfeld, J. H.: Secondary organic aerosol formation from cyclohexene ozonolysis: Effect of OH scavenger and the role of radical chemistry, Environ. Sci. Technol., 38, 3343–3350, 2004.
Kostenidou, E., Pathak, R. K., and Pandis, S. N.: An algorithm for the calculation of secondary organic aerosol density combining AMS and SMPS data, Aerosol Sci. Technol., 41, 1002–1010, 2007.
Koch, S., Winterhalter, R., Uherek, E., Kolloff, A., Neeb, P., Moortgat, G. K.: Formation of new particles in the gas-phase ozonolysis of monoterpenes, Atmos. Environ., 34, 4031–4042, 2000.
Kroll, J. H., Ng, N. L., Murphy, S. M., Flagan, R. C., and Seinfeld, J. H.: Secondary organic aerosol formation from isoprene photooxidation, Environ. Sci. Technol., 40, 1869–1877, 2006.
Kulmala, M., Vehkamäki, H., Petäjä, T., Dal Maso, M., Lauria, A., Kerminen, V.-M., Birmili, W., and McMurry, P. H.: Formation and growth rates of ultrafine atmospheric particles: A review of observations, J. Aerosol Sci., 35, 143–176, 2004.
Laaksonen, A., Kulmala, M., O'Dowd, C. D., Joutsensaari, J., Vaattovaara, P., Mikkonen, S.,

Lehtinen, K. E. J., Sogacheva, L., Dal Maso, M., Aalto, P., Petäjä, T., Sogachev, A., Yoon, Y. J., Lihavainen, H., Nilsson, D., Facchini, M. C., Cavalli, F., Fuzzi, S., Hoffmann, T., Arnold, F., Hanke, M., Sellegri, K., Umann, B., Junkermann, W., Coe, H., Allan, J. D., Alfarra, M. R., Worsnop, D. R., Riekkola, M.-L., Hyötyläinen, T., and Viisanen, Y.: The role of VOC oxidation products in continental new particle formation, Atmos. Chem. Phys., 8, 2657–2665, 2008, http://www.atmos-chem-phys.net/8/2657/2008/.

Lambe, A. T., Zhang, J. Y., Sage, A. M., and Donahue, N. M.: Controlled OH radical production via Ozone-alkene reactions for use in aerosol aging studies, Environ. Sci. Technol., 41, 2357–2363, 2007.

Lindfors, V. and Laurila, T.: Biogenic volatile organic compound (VOC) emissions from forests in Finland, Boreal Environ. Res., 5, 95–113, 2000.

Lindinger, W., Hansel, A., and Jordan, A.: Proton-transfer-reaction mass spectrometry (PTR-MS): On-line monitoring of volatile organic compounds at pptv levels, Chem. Soc. Rev., 27, 347–354, 1998.

Manninen, A.-M., Vuorinen, M., and Holopainen, J. K.: Variation in growth, chemical defense and herbivore resistance in Scots pine provenances. J. Chem. Ecol., 24, 1315–1331, 1998.

Mäntylä, E., Alessio, G. A., Blande, J. D., Heijari, J., Holopainen, J. K., Laaksonen, T., Piirtola, P., and Klemola, T.: From plants to birds: Higher avian predation rates in trees responding to insect herbivory, PLoS ONE 3, p. e2832, doi:10.1371/journal.pone.0002832, 2008.

McFiggans, G., Coe, H., Burgess, R., Allan, J., Cubison, M., Alfara, M. R., Saunders, R., Saiz-Lopez, A., Plane, J. M. C., Wevill, D., Carpenter, L., Rickard, A. R., and Monks, P. S.: Direct evidence for coastal iodine particles from Laminaria macroalgae – linkage to emissions of molecular iodine, Atmos. Chem. Phys., 4, 701–713, 2004, http://www.atmos-chem-phys.net/4/701/2004/.

Mentel, Th. F., Wildt, J., Kiendler-Scharr, A., Kleist, E., Tillmann, R., Dal Maso, M., Fisseha, R., Hohaus, Th., Spahn, H., Uerlings, R., Wegener, R., Griffiths, P. T., Dinar, E., Rudich, Y., and Wahner, A.: Photochemical production of aerosols from real plant emissions, Atmos. Chem. Phys. Discuss., 9, 3041–3094, 2009, http://www.atmos-chem-phys-discuss.net/9/3041/2009/.

Ng, N. L., Chhabra, P. S., Chan, A. W. H., Surratt, J. D., Kroll, J. H., Kwan, A. J., McCabe, D. C., Wennberg, P. O., Sorooshian, A., Murphy, S. M., Dalleska, N. F., Flagan, R. C., and Seinfeld, J. H.: Effect of NO_x level on secondary organic aerosol (SOA) formation from the photooxidation of terpenes, Atmos. Chem. Phys., 7, 5159–5174, 2007,

http://www.atmos-chem-phys.net/7/5159/2007/.
Niki, H., Maker, P. D., Savage, C. M., Breitenbach, L. P., and Hurley, M. D.: FTIR spectroscopic study of the mechanism for the gas-phase reaction between ozone and tetramethylethylene, J. Phys. Chem., 91, 941–946, 1987.
Odum, J. R., Hoffmann, T., Bowman, F., Collins, D., Flagan, R. C., and Seinfeld, J. H.: Gas/Particle partitioning and secondary organic aerosol yields, Environ. Sci. Technol., 30, 2580–2585, 1996.
Paulson, S. E., Sen, A. D., Liu, P., Fenske, J. D., and Fox, M. J.: Evidence of formation of OH radicals from the reaction of O_3 with alkenes in the gas phase, Geophy. Res. Lett., 24, 3193–3196, 1997.
Pinto, D. M., Tiiva, P., Miettinen, P., Joutsensaari, J., Kokkola, H., Nerg, A-M., Laaksonen, A., and Holopainen, J. K.: The effects of increasing atmospheric ozone on biogenic monoterpene profiles and the formation of secondary aerosols, Atmos. Environ., 41, 4877–4887, 2007.
Presto, A. A. and Donahue, N. M.: Secondary organic aerosol production from terpene ozonolysis. 2. Effect of NO_x concentration, Environ. Sci. Technol., 39, 7046–7054, 2005.
Räisänen, T., Ryyppö, A., and Kellomäki, S.: Effects of elevated CO_2 and temperature on monoterpene emission of Scots pine (*Pinus sylvestris* L.), Atmos. Environ., 42, 4160–4171, 2008.
Saathoff, H., Naumann, K.-H., Möhler, O., Jonsson, Å. M., Hallquist, M., Kiendler-Scharr, A., Mentel, Th. F., Tillmann, R., and Schurath, U.: Temperature dependence of yields of secondary organic aerosols from the ozonolysis of α-pinene and limonene, Atmos. Chem. Phys., 9, 1551–1577, 2009, http://www.atmos-chem-phys.net/9/1551/2009/.
Sakulyanontvittaya, T., Duhl, T., Wiedinmyer, C., Helmig, D., Matsunaga, S., Potosnak, M., Milford, J., and Guenther, A.: Monoterpene and sesquiterpene emission estimates for the United States, Environ. Sci. Technol., 42, 1623–1629, 2008.
Salcedo, D., Onasch, T. B., Dzepina, K., Canagaratna, M. R., Zhang, Q., Huffman, J. A., DeCarlo, P. F., Jayne, J. T., Mortimer, P., Worsnop, D. R., Kolb, C. E., Johnson, K. S., Zuberi, B., Marr, L. C., Volkamer, R., Molina, L. T., Molina, M. J., Cardenas, B., Bernabé, R. M., Márquez, C., Gaffney, J. S., Marley, N. A., Laskin, A., Shutthanandan, V., Xie, Y., Brune, W., Lesher, R., Shirley, T., and Jimenez, J. L.: Characterization of ambient aerosols in Mexico City during the MCMA-2003 campaign with Aerosol Mass Spectrometry: results from the

CENICA Supersite, Atmos. Chem. Phys., 6, 925–946, 2006, http://www.atmos-chem-phys.net/6/925/2006/.
Shilling, J. E., Chen, Q., King, S. M., Rosenoern, T., Kroll, J. H., Worsnop, D. R., McKinney, K. A., and Martin, S. T.: Particle mass yield in secondary organic aerosol formed by the dark ozonolysis of α-pinene, Atmos. Chem. Phys., 8, 2073–2088, 2008, http://www.atmos-chem-phys.net/8/2073/2008/.
Shilling, J. E., Chen, Q., King, S. M., Rosenoern, T., Kroll, J. H., Worsnop, D. R., DeCarlo, P. F., Aiken, A. C., Surper, D., Jimenez, J. L., and Martin, S. T.: Loading-dependent elemental composition of α-pinene SOA particles, Atmos. Chem. Phys., 9, 771–782, 2009, http://www.atmos-chem-phys.net/9/771/2009/.
Taipale, R., Ruuskanen, T. M., Rinne, J., Kajos, M. K., Hakola, H., Pohja, T., and Kulmala, M.: Technical Note: Quantitative long-term measurements of VOC concentrations by PTR-MS – measurement, calibration, and volume mixing ratio calculation methods, Atmos. Chem. Phys., 8, 6681–6698, 2008, http://www.atmos-chem-phys.net/8/6681/2008/.
Tarvainen, V., Hakola, H., Hellén, H., Bäck, J., Hari, P., and Kulmala, M.: Temperature and light dependence of the VOC emissions of Scots pine, Atmos. Chem. Phys., 5, 989–998, 2005, http://www.atmos-chem-phys.net/5/989/2005/.
Tsigaridis, K. and Kanakidou, M.: Global modeling of secondary organic aerosol in the troposphere: a sensitivity analysis, Atmos. Chem. Phys., 3, 1849–1869, 2003, http://www.atmos-chem-phys.net/3/1849/2003/.
Tuazon, E. C., Aschmann, S., Arey, J., and Atkinson, R.: Products of the gas-phase reactions of O_3 with a series methyl-substituted ethenes, Environ. Sci. Technol., 31, 3004–3009, 1997.
Tuazon, E. C., Aschmann, S, Arey, J., and Atkinson, R.: Products of the gas-phase reactions of a series of methyl-substituted ethenes with the OH radical, Environ. Sci. Technol., 32, 2106–2112, 1998.
VanReken, T. M., Greenberg, J. P., Harley, P. C., Guenther A. B., and Smith, J. N.: Direct measurement of particle formation and growth from the oxidation of biogenic emissions, Atmos. Chem. Phys., 6, 4403–4413, 2006, http://www.atmos-chem-phys.net/6/4403/2006/.
Vuorinen, T., Nerg, A.-M., Ibrahim, M. A., Reddy, G. V. P., and Holopainen, J. K.: Emission of *Plutella xylostella*-induced compounds from cabbages grown at elevated CO_2 and orientation behavior of the natural enemies, Plant Physiol., 135, 1984–1992, 2004.

Yu, J. Z., Cocker III, D. R., Griffin, R. J., Flagan, R. C., and Seinfled, J. H.: Gas-phase ozone oxidation of monoterpenes: Gaseous and particulate products, J. Atmos. Chem., 34, 207–258, 1999.

Zhang, Q., Stanier, C. O., Canagaratna, M. R., Jayne, J. T., Worsnop, D. R., Pandis, S. N., and Jimenez, J. L.: Insights into the chemistry of new particle formation and growth events in Pittsburgh based on Aerosol Mass Spectrometry, Environ. Sci. Technol., 38, 4797–4809, 2004.

Ziemann, P. J.: Formation of alkoxyhydroperoxy aldehydes and cyclic peroxyhemiacetals from reactions of cyclic alkenes with O_3 in the presence of alcohols, J. Phys. Chem. A, 107, 2048–2060, 2003.

Table 1. Gas phase kinetic constants, OH yield (Y_{OH}), acetone (AT) yield (Y_{AT}), formaldehyde (FAH) yield (Y_{FAH}) and correction factors used in the study.

VOCs	Rate constant, k (cm^3 $molecule^{-1}$ s^{-1})[a]	Y_{OH} (ω_i, ω'_i)[a,b]	Y_{AT} (β_i, β'_i)[c,d]	Y_{FAH} (α_i, α'_i)[c,e]	Correction factor (γ_i, γ'_i)	(γ''_i, γ'''_i)
TME+O_3	113×10^{-17}	1.0	1.05	0.28	1.0	–
TME+OH	110×10^{-12}	–	1.7	–	–	1.0
Isoprene+O_3	1.27×10^{-17}	0.27	–	0.9	1.1	–
Isoprene+OH	100×10^{-12}	–	–	0.63	–	1.2
Myrcene+O_3	47×10^{-17}	0.63	0.26	0.26	1.2	–
Mycrene+OH	215×10^{-12}	–	0.45	0.30	–	1.3
β-phellandrene+O_3	4.7×10^{-17}	0.14	–	–	1.1	–
β-phellandrene+OH	168×10^{-12}	–	–	–	–	1.2
Limonene+O_3	21×10^{-17}	0.67	0.02	0.02	1.1	–
Limonene+OH	164×10^{-12}	–	0.03	–	–	1.2
Δ^3-carene+O_3	3.7×10^{-17}	0.86	0.22	0.16	1.0	–
Δ^3-carene+OH	88×10^{-12}	–	0.15	0.21	–	1.1
α-pinene+O_3	8.4×10^{-17}	0.8	0.08	0.15	1.0	–
α-pinene+OH	52.3×10^{-12}	–	0.15	0.19	–	1.1
β-pinene+O_3	1.5×10^{-17}	0.35	0.04	0.65	1.0	–
β-pinene+OH	74.3×10^{-12}	–	0.13	0.45	–	1.1
Camphene+O_3	0.09×10^{-17}	0.18	–	–	1.0	–
Camphene+OH	52×10^{-12}	–	0.39	–	–	1.1
Sabinene+O_3	8.3×10^{-17}	0.33	0.03	–	1.0	–
Sabinene+OH	117×10^{-12}	–	0.19	–	–	1.2
Terpinolene+O_3	190×10^{-17}	1.0	0.50	–	1.1	–
Terpinolene+OH	225×10^{-12}	–	0.39	0.29	–	1.2
Acetone+OH	0.17×10^{-12}	–	–	–	–	1.0
Formaldehyde+OH	9.37×10^{-12}	–	–	–	–	1.0
2-butanol+OH	8.7×10^{-12}	–	–	–	–	1.0

[a] Atkinson and Arey (2003a)
[b] Aschmann et al. (2002); Lambe et al. (2007); Paulson et al. (1997)
[c] Atkinson and Arey (2003b)
[d] Tuazon et al. (1998)
[e] Grosjean et al. (1996)

Table 2. Initial conditions of chamber experiments performed and analysis results.

Date and year	Experiment No.	VOCs initial (ppb)	TME initial (ppb)	First O_3 addition				Second O_3 addition			
				Inlet (ppb)	time (min)*	Peak O_3 (ppb)**	Peak OH (ppt)***	Inlet (ppb)	time (min)*	Peak O_3 (ppb)**	Peak OH (ppt)***
12 Oct 2007	E1a	74.1	118	200	25	4.15	0.043	200	25	15.1	0.075
23 Oct 2007	E1b	28.8	342	200	75	5.17	0.073	0	0	0	0
25 Oct 2007	E1c	113.8	984	200	75	0	<0.0008	800	30	17.8	0.148
22 Oct 2007	E2	23.2	0	200	13	20.7	0.0139	0	0	0	0
26 Oct 2007	E3	100.3	2- butanol, 54 ppm	60	30	6.17	0.0001	200	30	37.4	0.0005

* Duration of ozone addition into the chamber.
** Measured maximum O_3 concentration inside the chamber.
***Modeled maximum OH concentration inside the chamber.

Table 3. Percentage molar contributions of different chemical compounds to pine emissions.

Pine VOCs (%)	E1a	E1b	E1c	E2	E3
α-pinene	26.3	27.1	30.4	26.7	47.4
β-pinene	1.5	3.4	28.4	3.4	7.6
Myrcene	11.9	11.8	8.8	16.4	4.6
β-phellandrene	8.0	16.7	4.5	20.2	4.4
Limonene	4.5	3.5	25.8	3.4	33.2
Δ^3-carene	40.4	30.9	0	22.0	0
Camphene	0.7	0.3	0.6	0.4	0.7
Sabinene	1.8	2.4	0	1.7	0
Terpinolene	1.8	1.7	0	1.7	0
Isoprene	3.0	2.1	1.3	3.9	2.0
Others	0.1	0.1	0.2	0.2	0.1

ACPD
9, 8223–8260, 2009

Table 4. Fraction by which each VOC react with OH during the first hour of new particle formation.

Fraction (VOC+OH, %)	α-pinene	β-pinene	Δ^3-carene	Limonene	Myrcene	Camphene	Sabinene	Terpinolene	β-phellandrene	Isoprene
E1a	81.3	97.2	94.3	84.5	76.2	99.8	90.8	45.3	96.2	98.2
E1b	86.1	98.0	95.9	88.6	81.9	99.8	93.3	54.0	97.3	98.7
E1c	85.8	98.0	/	88.3	81.6	99.8	/	/	97.2	98.7
E2	32.5	79.3	64.8	73.5	26.2	97.8	52.2	8.4	37.7	85.9
E3	1.2	8.8	/	1.5	0.9	52.8	/	/	6.5	13.2

Table 5. Effective density for different selected sizes of OH and O_3 induced SOA.

Chemical Systems	D_m (nm)	D_{va} (nm)	Effective density (g cm^{-3})
	76.1	101.8	1.34
OH+O_3	83.2	111.5	1.37
reactions	85.1	121.8	1.43
(E1 to E2)	104.2	133.7	1.28
	111.4	150.3	1.35
Average			1.34±0.06
	112.6	153.4	1.36
Ozonolysis	128.2	176.1	1.37
reactions	138.6	193.7	1.40
(E3)	155.9	212.4	1.36
	166.8	228.2	1.37
Average			1.38±0.03

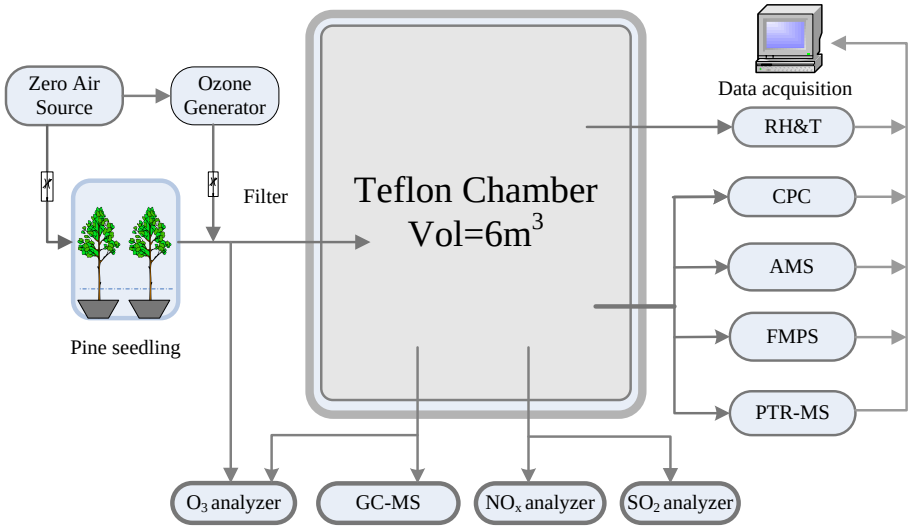

Fig. 1. Experimental schematic system used in these experiments.

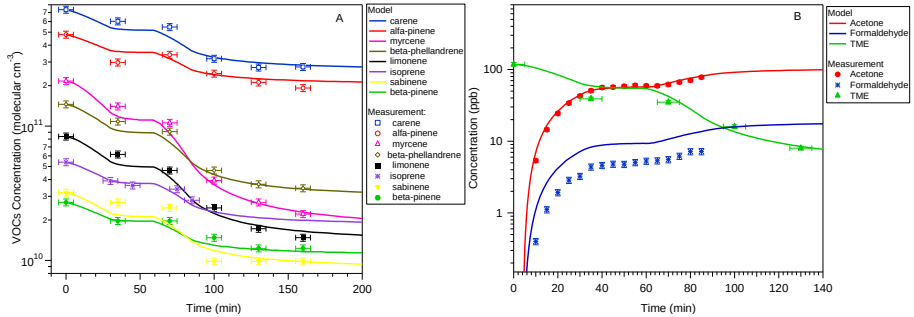

Fig. 2. Comparisions of measured and modelled results from experiment E1a: **(A)** Changes in emitted VOC concentration upon reaction (from GC-MS measurements) **(B)** TME decay profiles (from GC-MS measurements) and gas-phase product concentration of acetone and formaldehyde (from PTR-MS measurements). Results from other four experiments are similar and so are not be shown here.

ACPD
9, 8223–8260, 2009

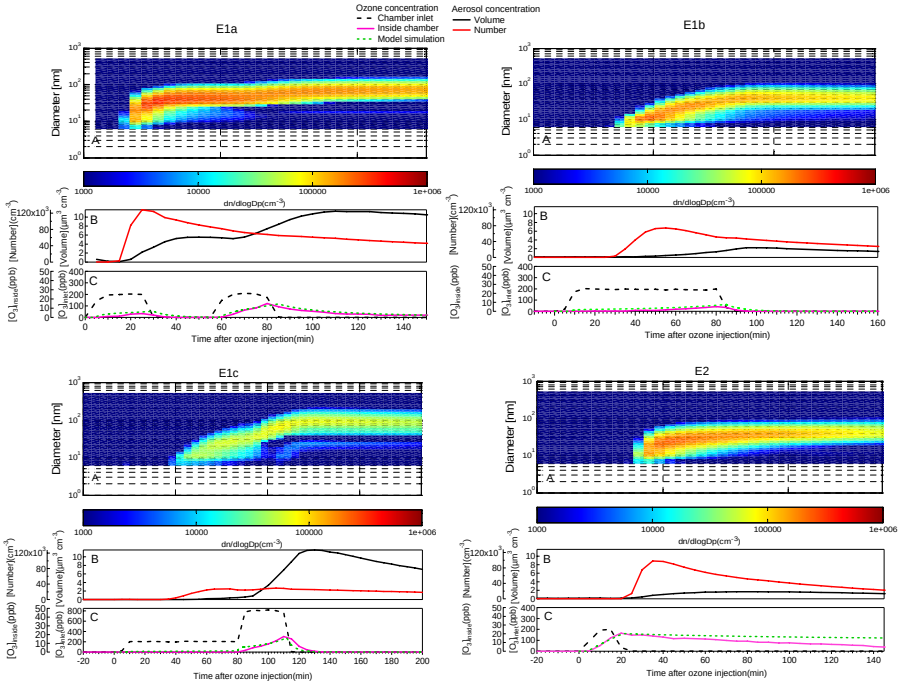

Fig. 3. New aerosol formations from OH and O_3-initiated oxidations of pine emissions. The frames contains from top to bottom, in order: **(A)** new particles size distributions plot, **(B)** measured aerosol number concentration (red curve) and volume concentration (black curve), and **(C)** measured ozone concentrations at the inlet (black dashed curve) and inside the chamber (pink curve) and modeled ozone concentration inside the chamber (green dashed curve).

ACPD
9, 8223–8260, 2009

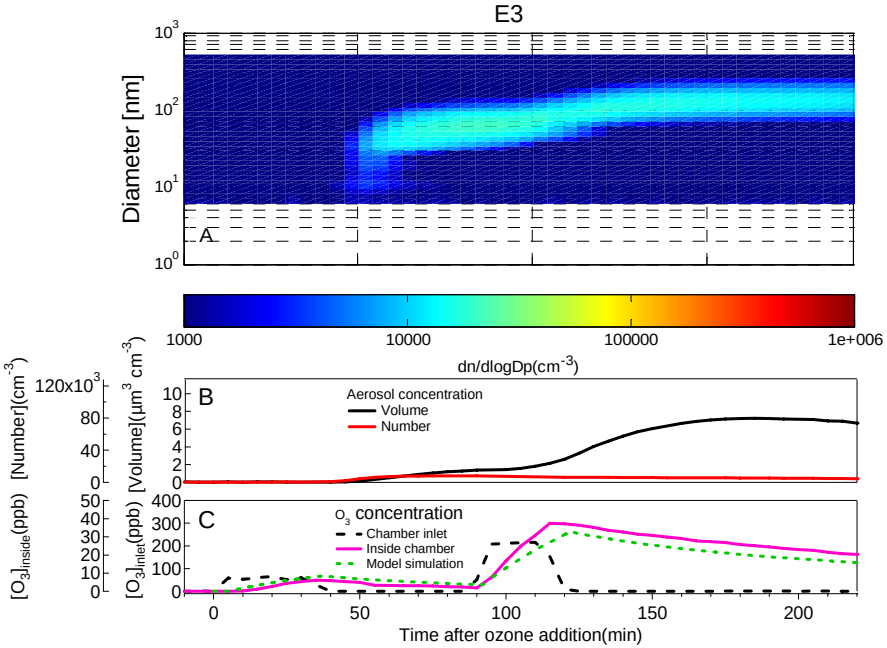

Fig. 4. New particle formations from ozonolysis of pine emissions in the presence of 2-butanol OH scavenger. The panel legends are the same as in Fig. 3.

ACPD
9, 8223–8260, 2009

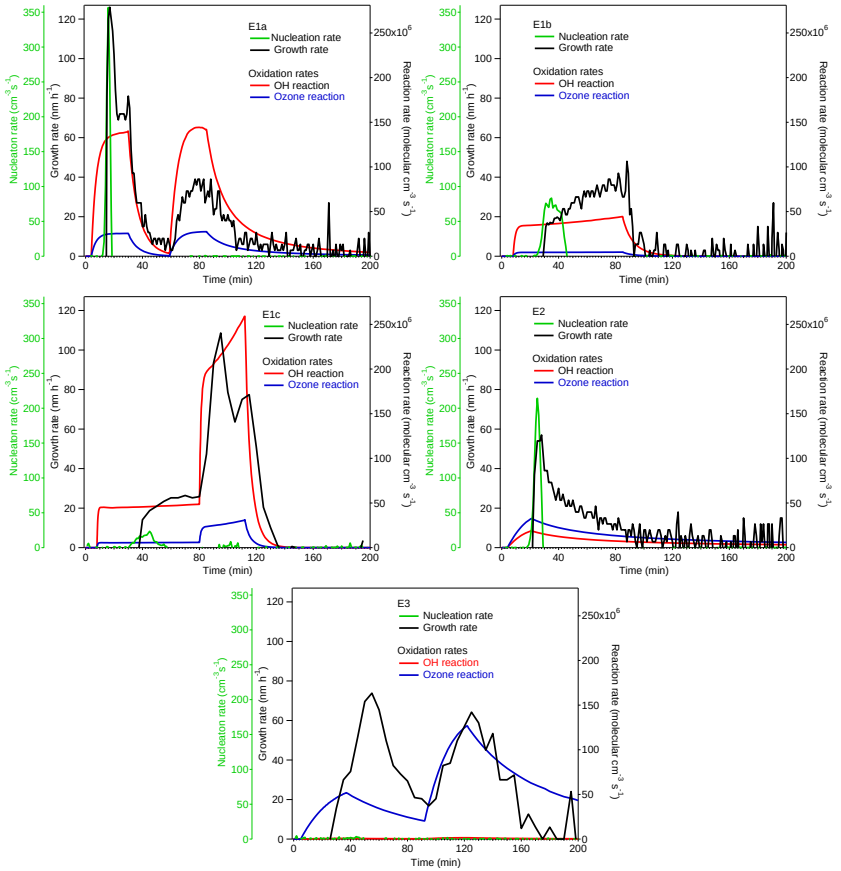

Fig. 5. Effects of ozonolysis and OH-initiated oxidation rates with emitted VOCs on new particle nucleation and growth rates. In these panels, nucleation and growth rates were determined from the FMPS size distributions data. OH and O_3 oxidation rates were calculated using the model described in Sect. 2.5.

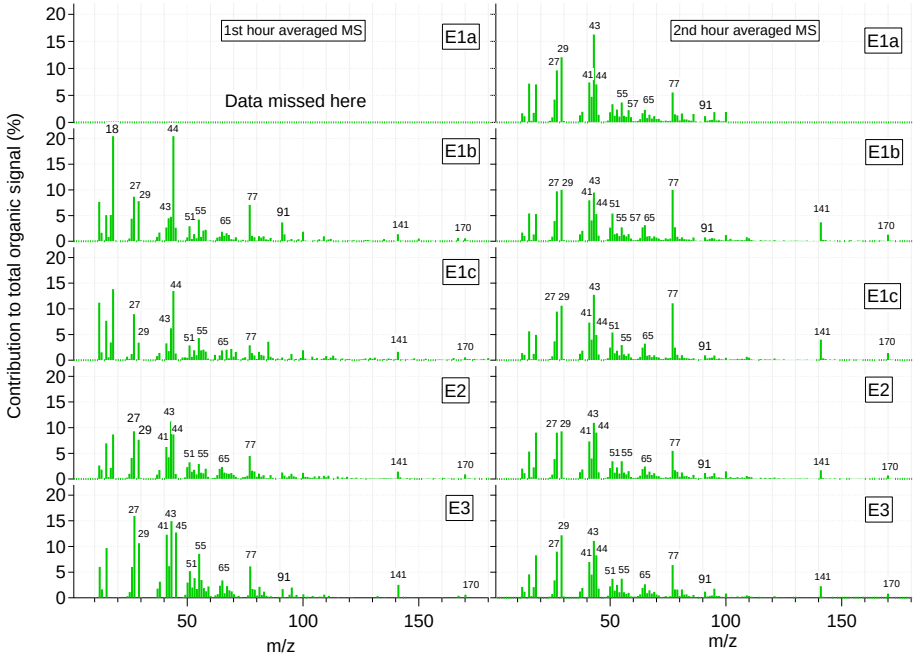

Fig. 6. Mass spectra of the aerosol products of the oxidation of pine VOCs from the first two hours of each experiment. All mass spectra are normalized to the sum total of all organic mass fragments, providing a quantitative fractional contribution of each mass fragment to the total measured signal. The left and right panels correspond to the mass spectra of the first and the second hours of reactions, respectively. In E1a, AMS scanned in the range of 1–100 amu, whereas the other four experiments scanned a wider range (1–200 amu), leading to small difference in percentage contributions in E1a. No AMS measurements were made in the first hour of experiment of E1a.